PREPARATION AND TESTING OF CORROSION- AND SPALLATION-RESISTANT COATINGS

Annual Topical Report

Reporting Period Start Date: October 1, 2013
Reporting Period End Date: September 30, 2014

Project Reporting Period: October 1, 2011 – September 30, 2015

Principal Author: John P. Hurley

Report Issue Date: October 2014
Cooperative Agreement No. DE-FE0007325

Submitting Organization:
Energy & Environmental Research Center
University of North Dakota
15 North 23rd Street, Stop 9018
Grand Forks, ND 58202-9018

John P. Hurley, Project Manager

October 2014

EERC DISCLAIMER

LEGAL NOTICE This research report was prepared by the Energy & Environmental Research Center (EERC), an agency of the University of North Dakota, as an account of work sponsored by the U.S. Department of Energy (DOE) National Energy Technology Laboratory. Because of the research nature of the work performed, neither the EERC nor any of its employees makes any warranty, express or implied, or assumes any legal liability or responsibility for the accuracy, completeness, or usefulness of any information, apparatus, product, or process disclosed or represents that its use would not infringe privately owned rights. Reference herein to any specific commercial product, process, or service by trade name, trademark, manufacturer, or otherwise does not necessarily constitute or imply its endorsement or recommendation by the EERC.

ACKNOWLEDGMENT

This material is based upon work supported by DOE under Award No. DE-FE0007325.

DOE DISCLAIMER

This report was prepared as an account of work sponsored by an agency of the United States Government. Neither the United States Government, nor any agency thereof, nor any of their employees, makes any warranty, express or implied, or assumes any legal liability or responsibility for the accuracy, completeness, or usefulness of any information, apparatus, product, or process disclosed, or represents that its use would not infringe privately owned rights. Reference herein to any specific commercial product, process, or service by trade name, trademark, manufacturer, or otherwise does not necessarily constitute or imply its endorsement, recommendation, or favoring by the United States Government or any agency thereof. The views and opinions of authors expressed herein do not necessarily state or reflect those of the United States Government or any agency thereof.

PREPARATION AND TESTING OF CORROSION- AND SPALLATION-RESISTANT COATINGS

ABSTRACT

This Energy & Environmental Research Center (EERC) project is designed to determine if plating APMT®, a specific highly oxidation-resistant oxide dispersion-strengthened FeCrAl alloy made by Kanthal, onto nickel-based superalloy turbine parts is a viable method for substantially improving the lifetimes and maximum use temperatures of the parts. The method for joining the APMT plate to the superalloys is called evaporative metal bonding and involves placing a thin foil of zinc (Zn) between the plate and the superalloy, clamping them together, and heating in an atmosphere-controlled furnace. Upon heating, the Zn melts and dissolves the oxide skins of the alloys at the bond line, allowing the two alloys to diffuse into each other. The Zn then diffuses through the alloys and evaporates from their surfaces.

Laboratory testing to determine the diffusion rate of Zn through the alloys has been completed. However, an analytical solution does not exist to model the diffusion of zinc through the alloys. For this reason, a finite difference algorithm using MATLAB was developed. It makes use of the hopscotch algorithm. The model allows the user to specify the dimensions of the metal parts, the Zn concentration at the bondline, the mesh size, time step, and Zn diffusivity. The experimentally measured values of diffusivity for Zn in APMT and Rene 80/CM 247LC are approximately 2.7×10^{-12} and 4×10^{-14} m^2/s, respectively.

While the qualitative behavior of the model appears correct, a comparison of the diffusion predictions with the experimental results from earlier in the project indicates that the expected Zn concentration is significantly higher than that measured experimentally. The difference depends on the assumed initial concentration, which is difficult to quantify exactly under experimental conditions for $t = 0$.

In addition to the diffusion work, the coefficients of thermal expansions were determined for each of the alloys as a function of temperature. This information has been entered into a finite element model using ANSYS so that appropriate force-applying structures can be designed for use in joining structures composed of APMT and the nickel alloys. Finite element modeling has been performed to finalize the fabrication geometry for the corrosion-testing phase. The addition of another bolt increases stress uniformity away from the region where the clamping is applied. It appears that a bolt spacing of approximately 25 mm in each jig is appropriate. This will allow the fabrication of 50-mm-wide sections of joints for the corrosion-testing task.

Gasifier sampling activities continue to determine what types of trace contaminants may occur in cleaned syngas that could lead to corrosion or deposition in turbines firing coal syngas. The EERC has several pilot-scale gasifiers that are continually used in a variety of test configurations as determined by the needs of the projects that are funding the tests. We are sampling both noncombusted and combusted syngas produced during some of the pilot-scale gasifier tests. This year sampling was performed of both syngas and combusted syngas while the entrained-flow gasifier (EFG) was firing subbituminous coal from the Antelope Mine in

Wyoming. Results of scanning electron microscope analyses of the syngas before combustion showed no submicron particles, only flakes of iron oxide that had likely formed on steel surfaces inside the combustor. As shown in the 2013 annual report, soot was also collected from the syngas when the much-lower-temperature fluid-bed gasifier (FBG) was fired, indicating that the much higher temperature of the EFG prevented soot formation. However, particles collected from the combusted syngas consist almost entirely of submicron soot, and little to no vaporized metals made it past the warm-gas filters and scrubbers in the high-temperature EFG system which could then deposit in a turbine system burning a higher hydrogen syngas. These results are consistent with the analyses of the particulates collected from combusted syngas when the lower-temperature FBG system is used.

TABLE OF CONTENTS

LIST OF FIGURES

LIST OF TABLES

PREPARATION AND TESTING OF CORROSION- AND SPALLATION-RESISTANT COATINGS

EXECUTIVE SUMMARY

This Energy & Environmental Research Center (EERC) project was designed to determine if plating APMT®, a specific highly oxidation-resistant oxide dispersion-strengthened FeCrAl alloy made by Kanthal, onto nickel-based superalloy turbine parts is a viable method for substantially improving the lifetimes and maximum use temperatures of the parts, both those with thermal barrier coatings and those without. The superalloys being investigated for protection are CM247LC and Rene® 80. Both are alumina-scale-forming alloys. The method for bonding the APMT plate to the superalloys is called evaporative metal bonding, which involves placing a thin foil of zinc (Zn) between the plate and the superalloy, clamping them together, and heating in an atmosphere-controlled furnace. Upon heating, the Zn melts and dissolves the oxide skins of the alloys at the bond line, allowing the two alloys to diffuse into each other. The Zn then diffuses through the alloys and evaporates from their surfaces.

If successful, the information developed will help move the protection process closer to demonstration testing. In addition, the team will characterize the microcontaminants in combusted higher-hydrogen-content gas. This information will be used to best simulate actual corrosion conditions in a turbine system and can also be used by other researchers studying deposition and gas flow in turbines.

Laboratory testing to determine the diffusion rate of Zn through the alloys has been completed. However, an analytical solution does not exist to model the diffusion of zinc through the alloys. For this reason, a finite difference algorithm using MATLAB was developed. It makes use of the hopscotch algorithm. The model allows the user to specify the dimensions of the metal parts, the Zn concentration at the bondline, the mesh size, time step, and Zn diffusivity. The experimentally measured values of diffusivity for Zn in APMT and Rene 80/CM 247LC are approximately 2.7×10^{-12} and 4×10^{-14} m^2/s, respectively.

While the qualitative behavior of the model appears correct, a comparison of the diffusion predictions with the experimental results from earlier in the project indicates that the expected Zn concentration is significantly higher than that measured experimentally. The difference depends on the assumed initial concentration, which is difficult to quantify exactly under experimental conditions for t = 0. However, it appears that the model predicts a concentration 2–3 times higher than that measured experimentally after 10 hours of diffusion. Additional investigations of this discrepancy are ongoing. This uncertainty in the model behavior is not expected to affect the ability to create good joints for the corrosion testing but will reduce confidence in being able to guarantee that the process has truly been optimized.

Additional finite element modeling has been performed to finalize the fabrication geometry for the corrosion-testing phase. The addition of another bolt increases stress uniformity away from the region where the clamping is applied. It appears that a bolt spacing of approximately

25 mm in each jig is appropriate. This will allow the fabrication of 50-mm-wide sections of joints for the corrosion-testing task.

In addition to the laboratory testing, gasifier sampling activities continue to determine what types of trace contaminants may occur in cleaned syngas that could lead to corrosion or deposition in turbines firing coal syngas. The EERC has several pilot-scale gasifiers that are continually used in a variety of test configurations as determined by the needs of the projects that are funding the tests. Under the University Turbine System Research (UTSR) Program, we are sampling both noncombusted and combusted syngas produced during some of the pilot-scale gasifier tests.

During the October to December 2013 quarterly reporting period, sampling was performed at both the inlet and the outlet of the TO_x while the entrained-flow gasifier (EFG) was firing subbituminous coal from the Antelope Mine in Wyoming. Results of SEM analyses of the syngas before combustion showed no submicron particles, only flakes of iron oxide that had likely formed on steel surfaces inside the combustor. As shown in the 2013 annual report, soot was also collected from the syngas when the much-lower-temperature fluid-bed gasifier (FBG) was fired, indicating that the much higher temperature of the EFG prevented soot formation. However, particles collected from the combusted syngas consist almost entirely of submicron soot, and little to no vaporized metals made it past the warm-gas filters and scrubbers in the high-temperature EFG system which could then deposit in a turbine system burning a higher hydrogen syngas. These results are consistent with the analyses of the particulates collected from combusted syngas when the lower-temperature FBG system was used.

NOMENCLATURE

APMT®	oxide dispersion-strengthened FeCrAl alloy made by Kanthal
ASME	American Society of Mechanical Engineers
CM247LC	alumina-scale-forming nickel-based superalloy
CVAAS	cold-vapor atomic absorption spectrometry
EDS	energy-dispersive spectroscopy
EFG	entrained-flow gasifier
EPA	U.S. Environmental Protection Agency
FBG	fluid-bed gasifier
Rene® 80	alumina-scale-forming nickel-based superalloy
SEM	scanning electron microscopy
UTSR	University Turbine System Research

PREPARATION AND TESTING OF CORROSION- AND SPALLATION-RESISTANT COATINGS

INTRODUCTION

The objective of this Energy & Environmental Research Center (EERC) project was to take a recently developed method of plating nickel superalloys with protective FeCrAl layers closer to commercial use in syngas-fired turbines. The project is designed to determine if plating APMT®, a specific highly oxidation-resistant oxide dispersion-strengthened FeCrAl alloy made by Kanthal, onto nickel-based superalloy turbine parts is a viable method for substantially improving the lifetimes and maximum use temperatures of the parts, both those with thermal barrier coatings (TBCs) and those without. The superalloys being investigated for protection are CM247LC and Rene® 80, both alumina-scale-forming alloys. The method for bonding the APMT plate to the superalloys is called evaporative metal bonding (EMB), which involves placing a thin foil of zinc (Zn) between the plate and the superalloy, clamping them together, and heating in an atmosphere-controlled furnace. Upon heating, the Zn melts and dissolves the oxide skins of the alloys at the bond line, allowing the two alloys to diffuse into each other. The Zn then diffuses through the alloys and evaporates from their surfaces.

If successful, the information developed will help move the protection process closer to demonstration testing. In addition, the team will characterize the microcontaminants in combusted higher-hydrogen-content gas. This information will be used to best simulate actual corrosion conditions in a turbine system and can also be used by other researchers studying deposition and gas flow in turbines.

EXPERIMENTAL METHODS

Laboratory Testing and Modeling

Under Tasks 2 and 3, we are measuring properties of the alloys and developing computer models of their high-temperature properties in order to develop the best methods for joining the APMT plate to CM247LC and Rene 80 turbine parts. In order to determine the best heating schedules to use for joining APMT plates to superalloy parts, we are measuring the diffusion rates of Zn through the alloys as a function of temperature. The experimental setup is described in last year's annual report. In order to develop the best clamp designs to use for holding the plating to the parts, we are measuring physical properties of the materials as a function of temperature.

Gasifier Sampling

In addition to the laboratory testing, we are continuing Task 4 sampling activities to determine what types of trace contaminants may occur in cleaned syngas that could lead to corrosion issues in turbines firing syngas. The EERC has two pilot-scale gasifiers that are intermittently used in a variety of test configurations. One is a pressurized entrained-flow gasifier (EFG), and the other is a pressurized fluid-bed gasifier (FBG). They are described in detail in the

2012 annual report. Funding for the actual operation of the gasifiers comes from projects other than this University Turbine System Research (UTSR) project. Particulates are collected by pulling approximately 1 cubic meter of gas through a cooled probe and through a Nucleopore filter with 0.1-μm holes.

RESULTS AND DISCUSSION

Laboratory Testing

The thermal expansion properties used for these calculations are slightly different for the Rene 80, CM247LC, and APMT than those reported in the Year 2 Quarter 3 report. It was discovered that oxidation had occurred on the thermomechanical analyzer (TMA) probe that may have affected the original results. The current calculations also include the actual measured values for the thermal expansion of the Mo jig. Prior calculations had assumed a constant value for the thermal expansion of the Mo (6×10^{-6} m/m) found in the literature. Measurements indicated the actual value to be more than twice this number at high temperatures. As a result, the maximum stresses at 1200°C are less than those reported previously (the higher thermal expansion of the Mo jig results in lower compressive stresses in the joint). Thermal expansion values used for each of the materials are shown in Table 1.

A review of studies that have investigated the effect of bonding pressure on diffusion bonding shows that joint strength tends to increase with bonding pressure up to a pressure in the low tens of MPa (1–4). At higher pressures, the resulting joint strength tends to decrease. No definitive explanation is available, but the consensus seems to be that the initial increase in joint strength is due to the flattening of surface asperities and more intimate contact between the mating surfaces. This increases the area available for diffusion. At some point, however, the

Table 1. Linear Coefficient of Thermal Expansion (α) as a Function of Temperature for Each Material Involved with the Bonding Process

Temperature, °C	APMT, 10^{-6}/°C	CM247LC, 10^{-6}/°C	Rene 80, 10^{-6}/°C	Mo, 10^{-6}/°C	Steel, 10^{-6}/°C
100	13.0	13.2	14.0	7.5	16.0
200	14.4	14.3	14.7	8.5	18.1
300	16.5	15.4	15.5	10.0	20.6
400	17.9	16.2	16.2	10.9	21.9
500	18.6	16.9	16.7	11.5	22.6
600	18.8	17.3	17.0	11.7	23.0
700	19.3	17.7	17.5	11.9	23.2
800	19.6	18.0	17.9	12.1	21.9
900	20.0	18.3	18.4	12.1	22.2
1000	20.5	18.3	19.1	13.3	22.5
1100	21.0	17.5	20.3	14.7	22.7
1200	21.2	16.9	21.3	15.2	23.0

asperities are flattened, and the pressure actually retards diffusion in the bonding region. Based on these results, it is desirable that the compressive stress at the joint interface remain above about 20 MPa.

Figure 1 shows the expected high-temperature strength of TZM Mo (5). At a bonding temperature of 1200°C (1473K), the expected yield strength of the jig material is approximately 400 MPa.

Using the von Mises equivalent stress criterion (6), the yield strength of a material under pure shear loading is 0.577 times the tensile yield strength. Thus the shear yield strength of the TZM Mo at 1200°C is approximately 230 MPa. Both the tensile and shear strengths are required to analyze the jig geometry. Most of the jig will be under either tensile loading or bending. However, the threads of the TZM Mo bolt and the jig hole will be loaded in shear because of thermal expansion. Table 2 shows additional high-temperature data for TZM Mo, including elongation and ultimate tensile strength (7).

The jig geometry used for analysis of the diffusion process had a cross-sectional area in the walls of 475 mm^2 (2 × 12.5 mm × 19 mm). If a load of 200 kN is applied to this area, this results in a normal stress of approximately 420 MPa. Based on the information in Figure 1 and Table 1, at this stress level, the Mo jig would be expected to plastically deform. But no plastic deformation was observed in the jig after bonding. There are two possible explanations: 1) the finite element analysis (FEA) stress predictions are incorrect or 2) there is additional deformation happening in the experimental samples that is not accounted for in the FEA model that leads to an overall stress reduction in the Mo.

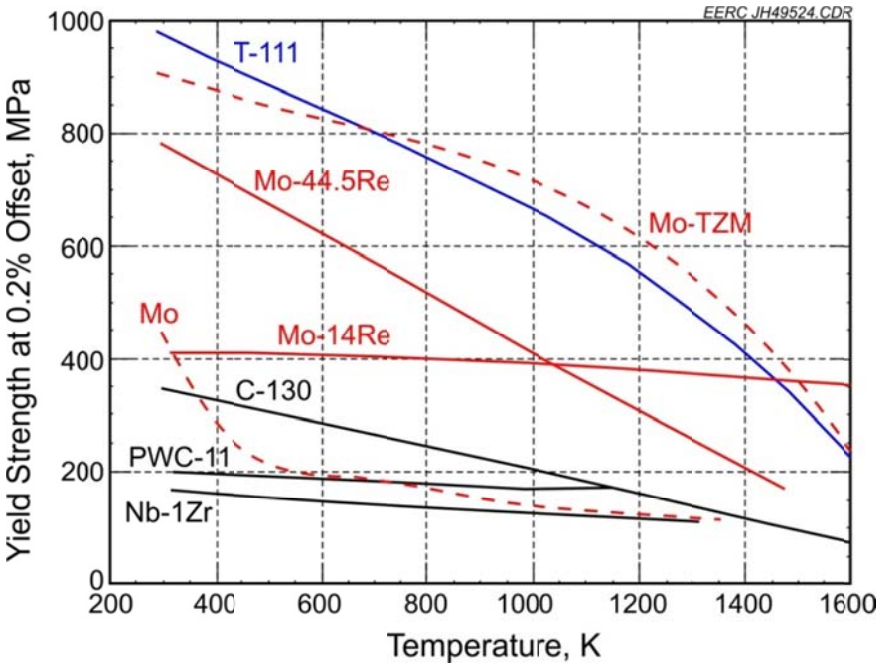

Figure 1. Variation of yield strength of various Mo and high-temperature alloys with temperature (5).

Table 2. Strength and Elongation Data for TZM Mo as a Function of Temperature and Rolling Direction (3)

Temperature, °C	Yield Stress, MPa	Ultimate Tensile Strength, MPa	Total Elongation, %	Uniform Elongation, %	Reduction in Area, %	Young's Modulus, GPa
Longitudinal (LSR) Data						
−194	NA[1]	1455	0	0	0	
−150	NA	1436±73	1±1	0±0	3	
−100	1224±33	1232±26	1.9±1.7	0.7±0.1	7	312±18
−50	1033±33	1041±33	8.11±5.4	4.2±3.2	29±14	
RT[2]	730±32	808±34	16.3±3.1	9.2±2.7	47±11	291±18
100	650±19	756±30	12.3±1.7	6.5±1.3	65	273±3
200	577±12	674±18	9.0±0.9	4.7±1.5	61	250±8
300	600	669	8.0	1.9	70	
400	615	673	7.0	2.6	69	
600	572±3	628±14	4.8±0.2	2.2±0.3		242±9
702	510	556	5.0	1.6	75	
800	497±21	539±38	4.0±0.5	1.9±0.1		243±3
976	448	487	5.0	1.6	>99	
1000	489±19	524±16	3.6±0.4	1.5±0.4		223±18
1201	402	414	7	7	86	
1406	107	172	30	30	97	
Transverse (TSR) Data						
−194	NA	1390	0	0	0	
−150	NA	1536	<1	<1	0	
−100	1328±22	1333±14	0.8±0.2	0.6±0.0	0	326±5
−50	1170±56	1155±61	4.3±2.9	0.6±0.1	13	319±3
0	895	929	11	6	40	
RT	810±43	852±27	11.7±1.7	5.4±0.5	36	294±15
100	761±23	815±18	8.6±2.2	4.2±1.1	47	296±0
200	662±38	721±27	6.3±1.1	3.5±0.6	55	270±17
300	652	694	5	3	61	
400	607	648	6	2	68	
600	637±9	670±20	2.5±0.4	1.0±0.1		268±7
701	544	611	4.0	1.0	59	
800	575±26	600±24	2.7±0.4	0.8±0.1		242±1
1000	550±34	570±35	2.6±0.4	0.9±0.1		223±15

[1] Not analyzed.
[2] Room temperature.

Modeling

Figure 2 shows the diffusion conditions experienced by joints during the evaporative bonding process. "Initial" and "boundary" refer to the type of condition. The schematic makes use of symmetry about the midline of the zinc layer.

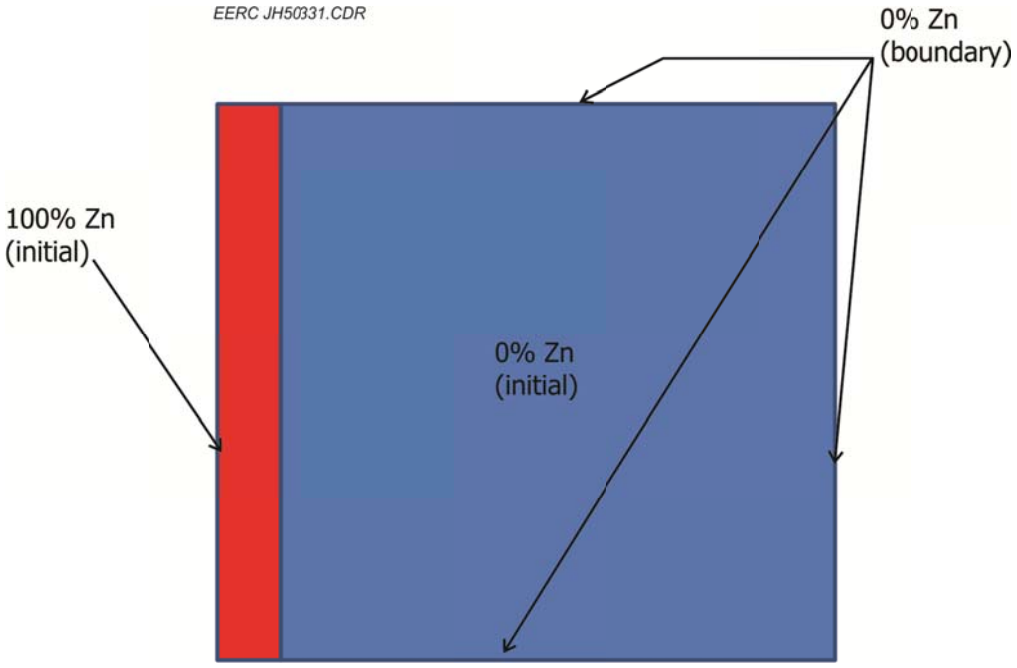

Figure 2. Diffusion conditions during evaporative metal bonding.

Equation 1 is the three-dimensional diffusion equation for a constant diffusivity, D, where C is the concentration of the diffusing species; t is time; and x, y, and z are spatial coordinates.

$$\frac{\partial C}{\partial t} = D\left[\frac{\partial^2 C}{\partial x^2} + \frac{\partial^2 C}{\partial y^2} + \frac{\partial^2 C}{\partial z^2}\right] \quad \text{Eq. 1}$$

An analytical solution does not exist for Equation 1 for the conditions illustrated in Figure 2. For this reason, the setup shown in Figure 1 was implemented into a finite difference algorithm using MATLAB. It makes use of the hopscotch algorithm of Gourlay (8) and Gourlay and McGuire (9). The model allows the user to specify the dimensions of the metal parts, the Zn concentration at the bondline, the mesh size, time step, and Zn diffusivity. Figure 3 shows the predicted concentration at the bondline as a function of time for varying values of D. The experimentally measured values of D for Zn in APMT and Rene 80/CM 247LC are approximately 2.7×10^{-12} and 4×10^{-14} m^2/s, respectively.

While the qualitative behavior of the model appears correct, a comparison of the diffusion predictions from Figure 3 with the experimental results of Braband from earlier in the project (10), indicates that the expected Zn concentration is significantly higher than that measured experimentally. The difference depends on the assumed initial concentration, which is difficult to quantify exactly under experimental conditions for t = 0. However, it appears that the model predicts a concentration 2–3 times higher than that measured experimentally after 10 hours of diffusion. Additional investigations of this discrepancy are ongoing. This uncertainty in the model behavior is not expected to affect the ability to create good joints for the corrosion testing but will reduce confidence in being able to guarantee that the process has truly been optimized.

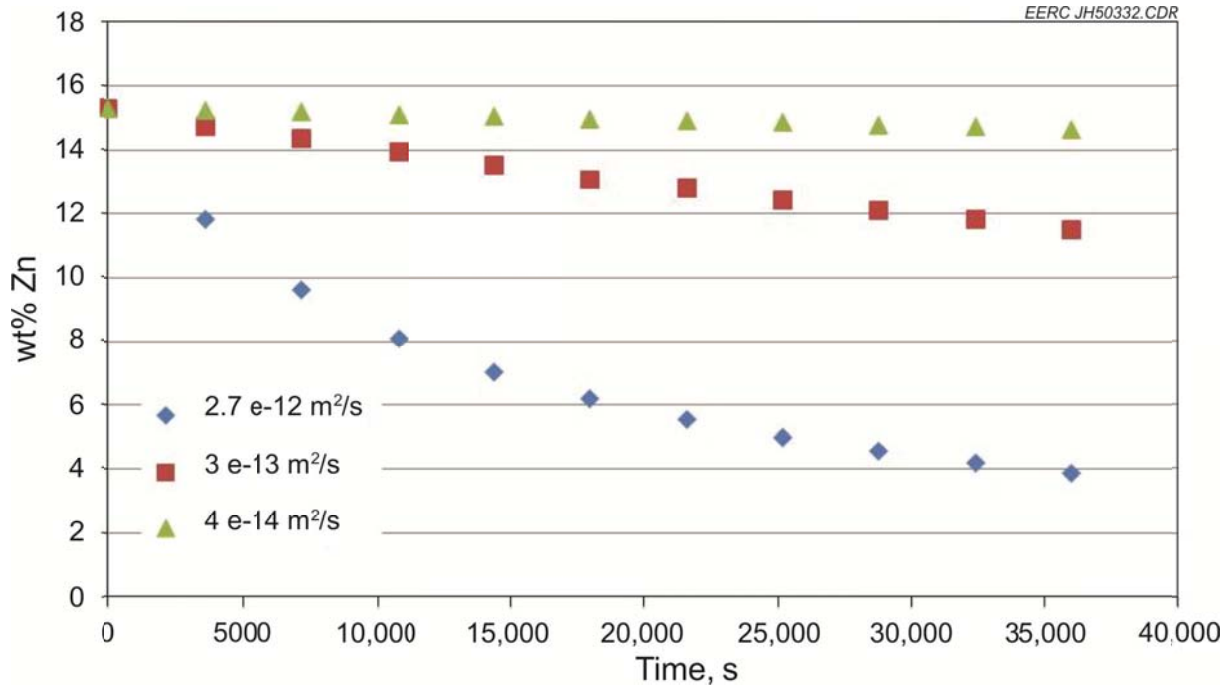

Figure 3. Predicted Zn concentration at the bondline with the base metal as a function of time.

Additional finite element modeling has been performed to finalize the fabrication geometry for the corrosion-testing phase. Prior reported results (April through June 2012 report) are repeated in Figures 4–6. Figures 7–9 show results for an alternate geometry in which the steel hemisphere has been removed and an additional TZM Mo bolt has been added. The addition of another bolt increases stress uniformity away from the region where the clamping is applied. It appears that a bolt spacing of approximately 25 mm in each jig is appropriate. This will allow the fabrication of 50-mm-wide sections of joints for the corrosion-testing task.

Figure 9 also shows very high stresses developed in the TZM Mo bolts when the steel hemispheres are not present. At 1200°C, the yield stress for TZM Mo is expected to be in range of 400 MPa. Both the bolts and the main jig have regions that experience stresses at or above this level. These stress levels were not observed in the previous geometry when the steel hemispheres were presented. Because the high-temperature yield strength of the steel is significantly lower, the presence of the spheres serves to both distribute the load and to reduce the maximum stress level in the jig. Thus even though the hemispheres are not expected to be required for alignment purposes when larger sections are fabricated, they will be retained because of their role in protecting the jig from permanent deformation.

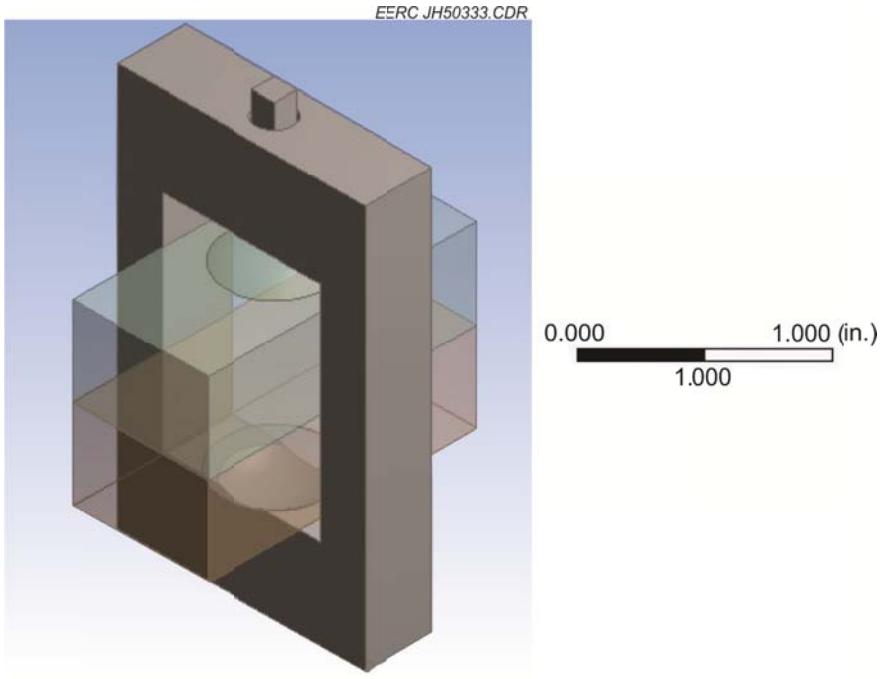

Figure 4. Isometric view of the joint model corresponding to the stress distributions in Figures 4 and 5.

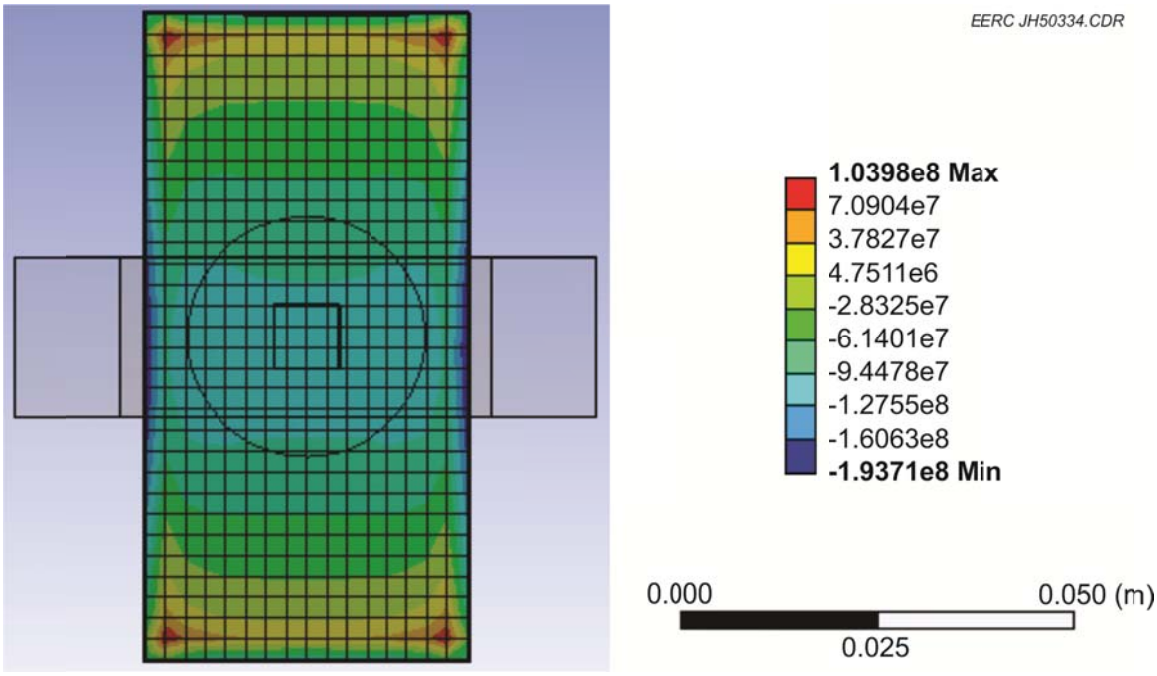

Figure 5. Finite element prediction of compressive stresses at the interface of CM 247/APMT at a temperature of 1200°C (no preload). Stress units are Pa.

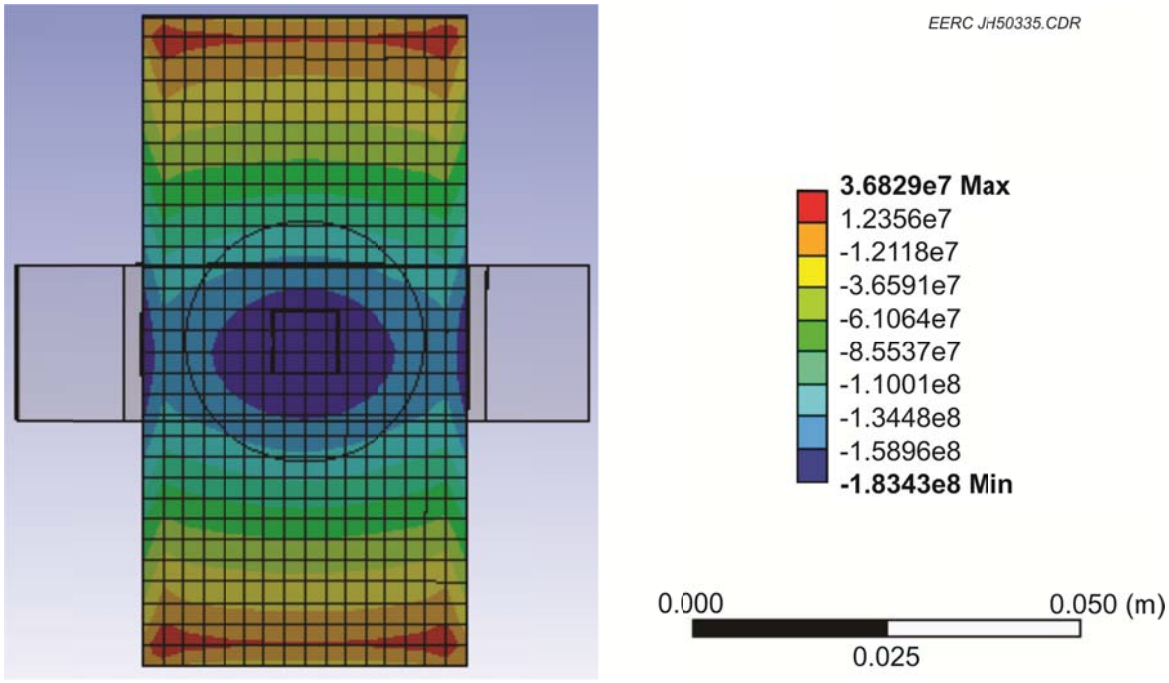

Figure 6. Finite element prediction of compressive stresses at the interface of Rene 80/APMT at a temperature of 1200°C (no preload). Stress units are Pa.

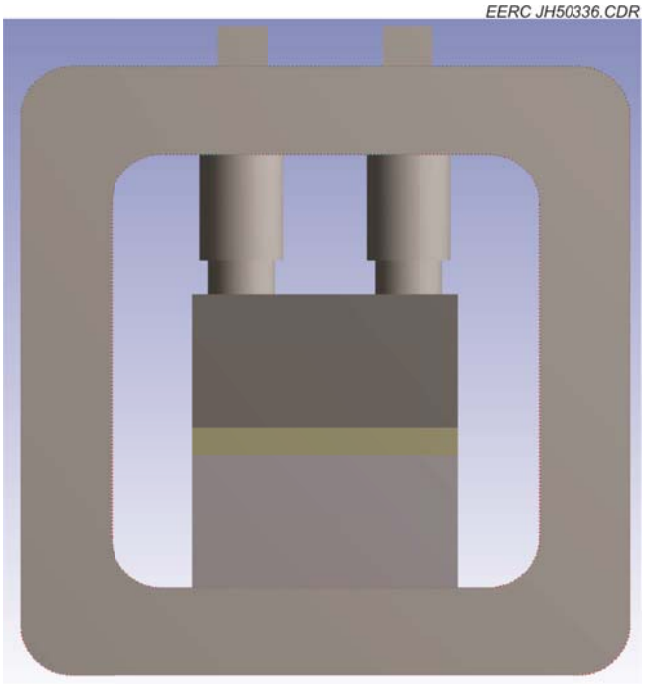

Figure 7. Alternate joint configuration with two bolts and without steel hemisphere.

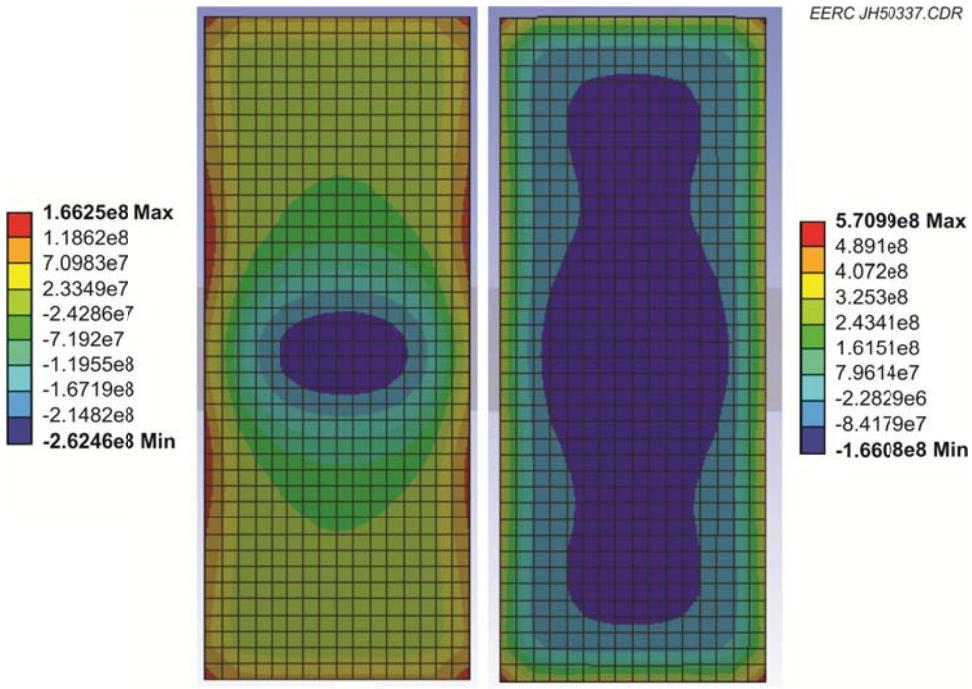

Figure 8. Predicted normal stresses at the APMT/base metal interface at 1200°C for the two-bolt jig geometry for a) Rene 80 and b) CM 247.

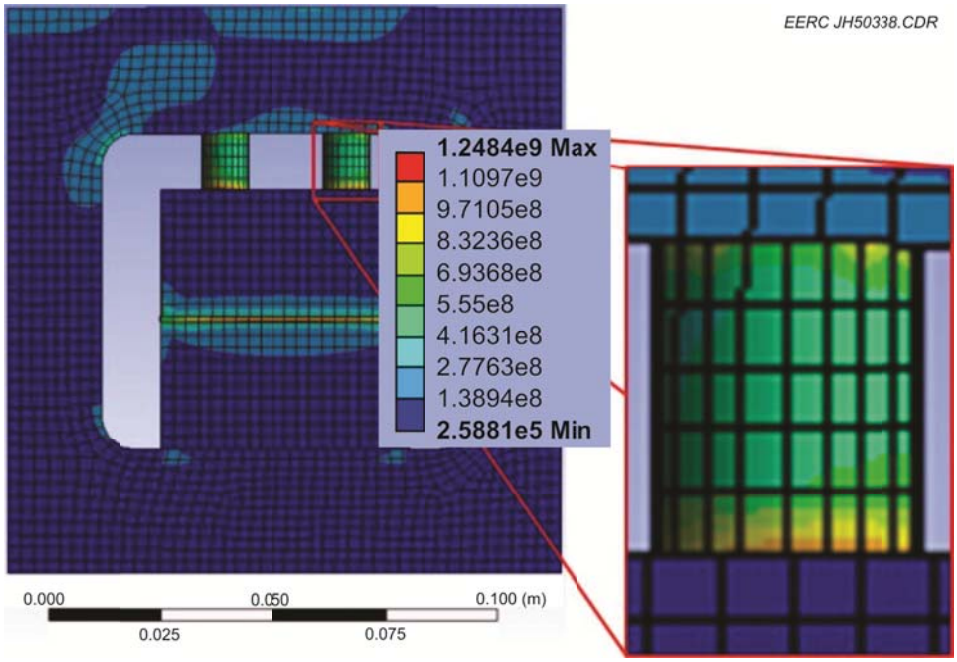

Figure 9. Equivalent (von Mises) stresses throughout the joint at 1200°C – expanded section shows stresses exceeding yield strength of TZM Mo in the bolts.

Gasifier Sampling

In addition to the laboratory testing and modeling, Task 4 gasifier sampling activities continue to determine what types of trace contaminants may occur in cleaned syngas that could lead to corrosion or deposition in turbines firing coal syngas. The EERC has several pilot-scale gasifiers that are continually used in a variety of test configurations as determined by the needs of the projects that are funding the tests. Under the UTSR Program, we are sampling both noncombusted and combusted syngas produced during some of the pilot-scale gasifier tests. The pressurized EFG was described in the January–March 2012 quarterly report, and the pressurized FBG was described in the April–June 2012 quarterly report. The thermal oxidizer used to combust the syngas contains a burner at the top of a refractory-lined chamber that admits the syngas and air separately and also includes a premixed natural gas and air supplemental gas stream. An accurate flame temperature is not available for the thermal oxidizer because thermocouples burn out too quickly in the flame. Particulates are collected from the syngas before the burner and from the combusted syngas at the bottom of the downfired oxidizer. The gas being sampled at the bottom is at approximately 750°C. It is quenched as it is pulled through the glass sampling tube to approximately 100°C before reaching the filter. The sampling train consists of a cooled one-piece glass nozzle–probe liner leading to a polycarbonate filter (Whatman™ Nucleopore™ type) with 0.1-μm holes. The gas and particulate sample are withdrawn nonisokinetically from the source.

During the October to December 2013 quarterly reporting period, sampling was performed at both the inlet and the outlet of the TO_x while the EFG was firing subbituminous coal from the Antelope Mine in Wyoming. Three samples were collected: one at the inlet of the TO_x and two at the outlet. The first sample was collected on October 29 at the outlet while coal syngas was being fired; the second was collected on October 30 from the coal syngas at the inlet to the TO_x; and the third sample was collected on November 4 at the TO_x outlet while firing on natural gas only. During these sampling periods, a total syngas volume of 153.25 ft^3 was collected in the sampling train with 56.8 ft^3 (1.61 m^3) for the first sample, 49.0 ft^3 (1.39 m^3) for the second, and 47.5 ft^3 (1.34 m^3) for the third. Particulate loadings were 0.808 mg/m^3 at the TO_x outlet when syngas was fired, 6.906 mg/m^3 at the TO_x inlet, and 0.698 mg/m^3 at the TO_x outlet when only natural gas was fired.

Initial analyses of the particles with the EERC JEOL 5800 scanning electron microscope (SEM) were reported in the April through June 2014 quarterly technical progress report. However, that SEM has relatively low resolution, so it was decided to repeat the analyses using a new high-resolution SEM on the University of North Dakota (UND) campus. Those analyses are now complete. The new UND field emission SEM is an FEI Quanta 650 FEG. The samples analyzed were cut from the filter and mounted on a carbon plug using carbon paint to hold them to the plugs. The samples were lightly coated with evaporated carbon to increase the electrical conductivity of their surfaces. Figure 10 shows the particles collected at the outlet of the TO_x while syngas and natural gas were being fired in the TO_x. The particles are primarily 0.05 to 0.2 μm in diameter. Energy- dispersive spectroscopy (EDS) of individual particles indicates that they all consist of approximately 89% carbon, 9% oxygen, and 1% nitrogen. Although we can expect that the EDS results would be heavily contaminated by x-rays from the filter (polycarbonate), we should have seen some signals from any metals that were present, indicating

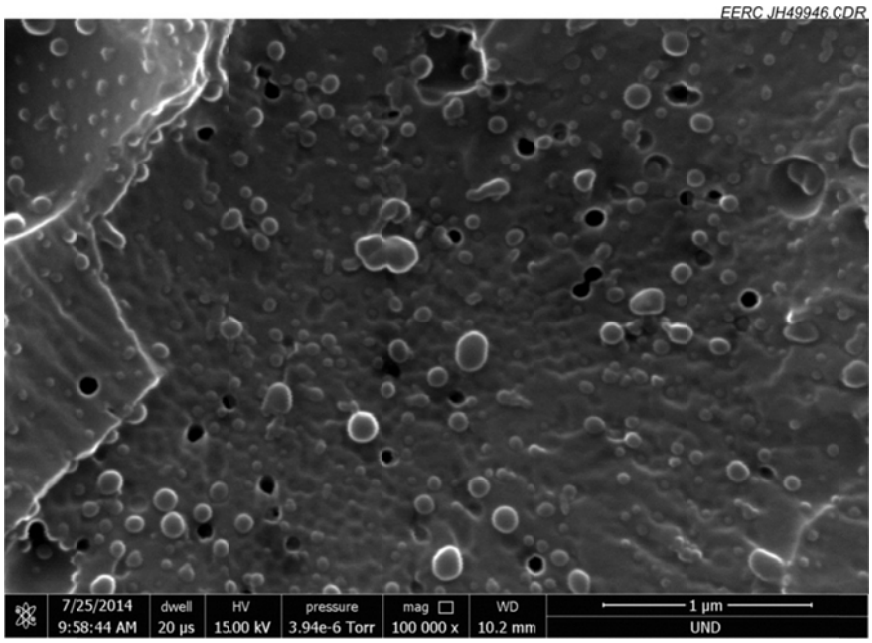

Figure 10. Particles collected at the outlet of the TO_x while syngas and natural gas were being fired in the TO_x.

that they are essentially all soot particles and not formed from vaporized metals that condensed in the cooler syngas stream. This is consistent with the results reported in the July to September 2013 quarterly technical progress report for particles collected from the system while an FBG was fired which were also essentially soot. This indicates that little to no vaporized metals made it past the warm-gas filters and scrubbers in the gasifier system.

Figure 11 shows particles collected at the inlet to the TO_x which were present in the unburned syngas. Even though this filter showed the highest weight gain during sampling, essentially no soot particles were found on the surface of the filter. However, there were large flakes of iron oxide containing some sodium, chlorine, sulfur, and zinc. Figure 12 shows one of these flakes. It is 200 µm long and 100 µm across. The flakes are what make up the weight gain measured for the filter. The lack of submicron soot particles is likely due to the very high operating temperature (1800°C) of the EFG, which reduces both soot and tar formation. Note, however, that soot particles do form during combustion of the syngas in TO_x, as shown in the last quarterly report.

Figure 13 shows particles collected at the outlet of the TO_x while it was burning only natural gas. These particles are smaller than those collected from the syngas at the TO_x outlet (according to their current labels) but, like those particles, consist only of carbon, oxygen, and a small amount of nitrogen.

These results indicate that the particles that were collected consist almost entirely of submicron soot and that little to no vaporized metals made it past the warm-gas filters and scrubbers in the high-temperature EFG system which could then deposit in a turbine system

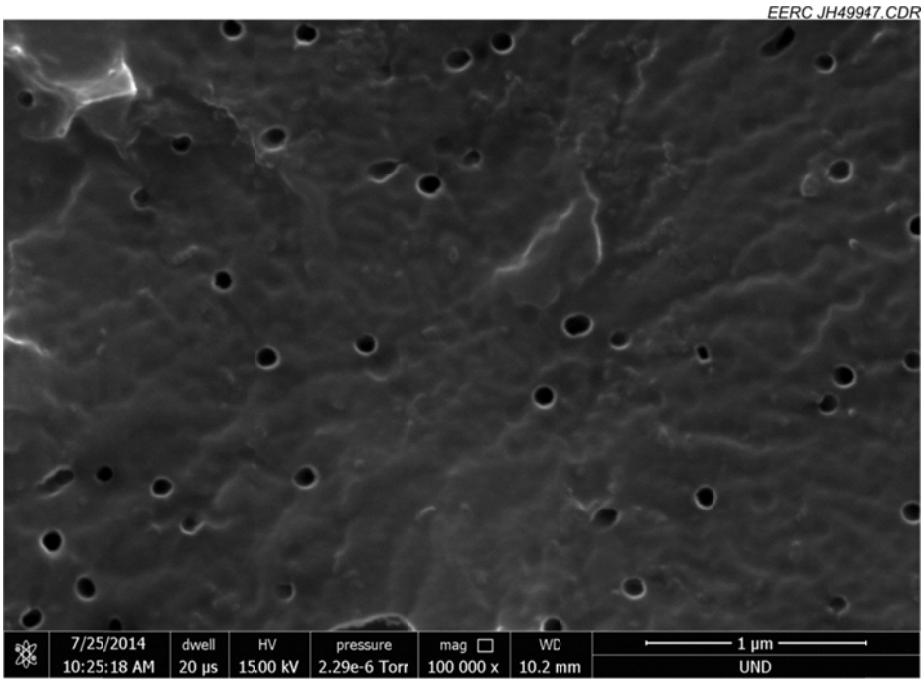

Figure 11. Particles collected at the inlet to the TO_x which were present in the unburned syngas.

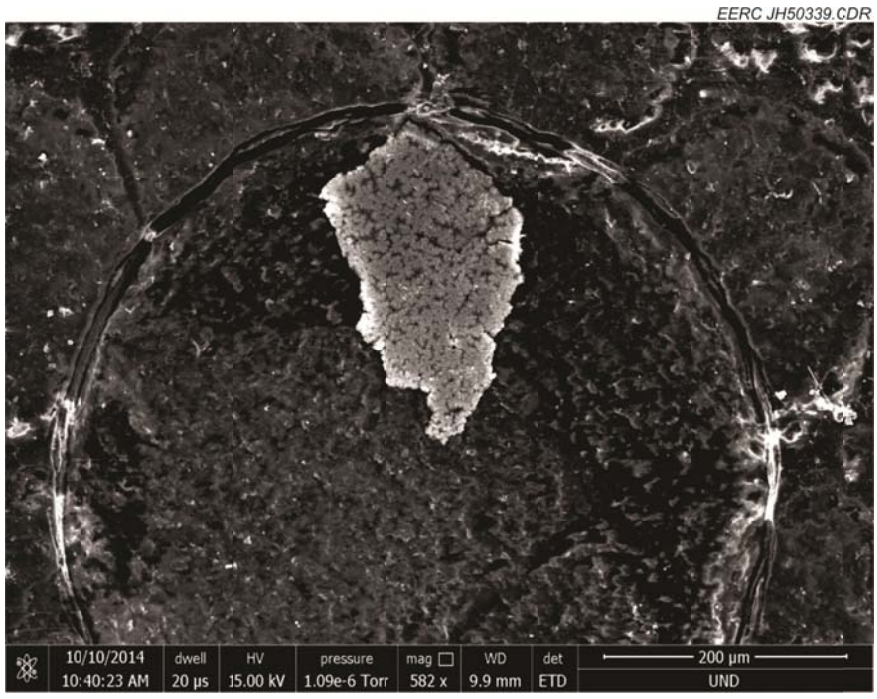

Figure 12. Large flake of iron oxide collected at the inlet of the TO_x.

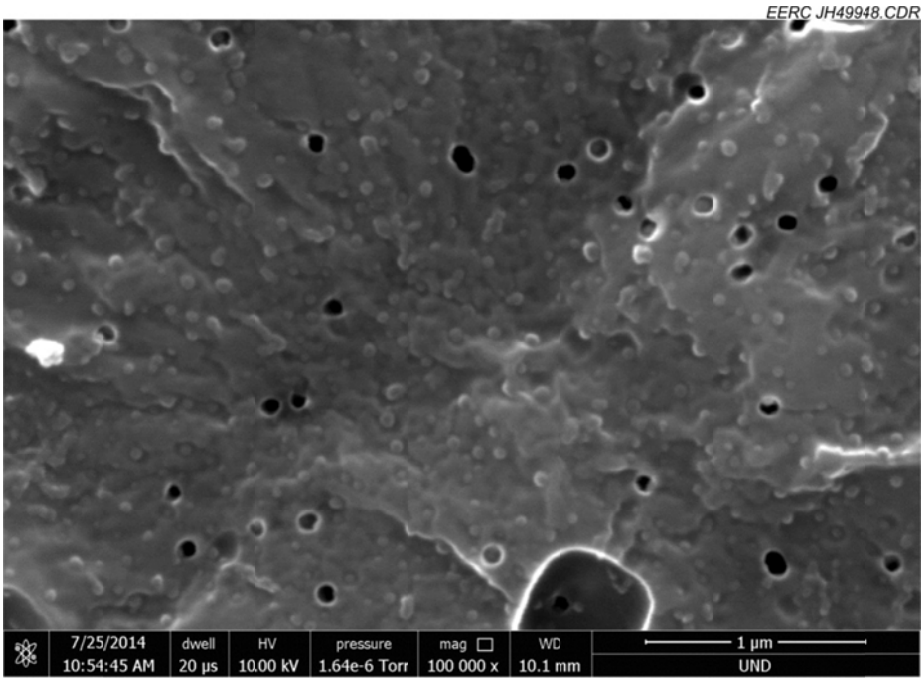

Figure 13. Particles collected at the outlet of the TO_x while it was burning only natural gas.

burning a higher hydrogen syngas. In addition, there were large flakes of iron oxide that likely formed on gasifier steel surfaces that could reach the turbine combustor. These results are consistent with the analyses of the particulates collected when the lower-temperature FBG system is used.

CONCLUSIONS

An analytical solution does not exist to model the diffusion of zinc through the alloys. For this reason, a finite difference algorithm using MATLAB was developed. While the qualitative behavior of the model appears correct, a comparison of the diffusion predictions with the experimental results from earlier in the project indicates that the expected Zn concentration is significantly higher than that measured experimentally. The difference depends on the assumed initial concentration, which is difficult to quantify exactly under experimental conditions for $t = 0$.

In addition to the diffusion work, the coefficients of thermal expansions were determined for each of the alloys as a function of temperature. This information has been entered into a finite element model using ANSYS so that appropriate force-applying structures can be designed for use in joining structures composed of APMT and the nickel alloys. Finite element modeling has been performed to finalize the fabrication geometry for the corrosion-testing phase. The addition of another bolt increases stress uniformity away from the region where the clamping is applied. It appears that a bolt spacing of approximately 25 mm in each jig is appropriate. This will allow the fabrication of 50-mm-wide sections of joints for the corrosion-testing task.

Gasifier sampling activities continue to determine what types of trace contaminants may occur in cleaned syngas that could lead to corrosion or deposition in turbines firing coal syngas. This year sampling was performed of both syngas and combusted syngas while the EFG fired subbituminous coal from the Antelope Mine in Wyoming. Results of SEM analyses of the syngas before combustion showed no submicron particles, only flakes of iron oxide that had likely formed on steel surfaces inside the combustor. As shown in the 2013 annual report, soot was also collected from the syngas when the much-lower-temperature FBG was fired, indicating that the much higher temperature of the EFG prevented soot formation. However, particles collected from the combusted syngas consisted almost entirely of submicron soot, and little to no vaporized metals made it past the warm-gas filters and scrubbers in the high-temperature EFG system which could then deposit in a turbine system burning a higher hydrogen syngas. These results are consistent with the analyses of the particulates collected from combusted syngas when the lower-temperature FBG system was used.

REFERENCES

1. Masahashi, N; Hanada, S. Effect of Pressure Application by HIP on Microstructure Evolution During Diffusion Bonding. *Materials Transactions* **2005**, *46* (7), 1651–1655.

2. Mahendran, G.; Babu, S.; Balasubramanian, V. Analyzing the Effect of Diffusion Bonding Process Parameters on Bond Characteristics of Mg-Al Dissimilar Joints. *Journal of Materials Engineering and Performance* **2010**, *19*, 657–665.

3. Kadhim, Z.D.; Al-Azzawi, A.I.; Al-Janabi, S.J. Effect of the Diffusion Bonding Conditions on Joint Strength. *Journal of Engineering and Development* **2009**, *13* (1), 179–188.

4. Al-Ajaj, E.A.; Awfa, A.R.; Ahmed, A.; Moosa, A. Modeling and Experimental Studies of Diffusion Bonding of Inconel 600 to Pyrolytic Graphite. *International Journal of Metallurgical and Materials Science and Engineering* **2013**, *3* (1), 9–30.

5. El-Genk, M.S.; Tournier, J.-M. A Review of Refractory Metal Alloys and Mechanically Alloyed Oxide Dispersion-Strengthened Steels for Space Nuclear Power Systems. *J. Nuclear Materials* **2005**, *340*, 93–112.

6. Dieter, G.E. *Mechanical Metallurgy;* McGraw-Hill: Boston, MA, 1986; Chapter 3.

7. Cockeram, B.V. The Mechanical Properties and Fracture Mechanisms of Wrought Low-Carbon Arc Cast (LCAC), Molybdenum-0.5pct Titanium-0.1pct Zirconium (TZM), and Oxide Dispersion-Strengthened (ODS) Molybdenum Flat Products. *Materials Science and Engineering A* **2006**, *418*, 120–136.

8. Gourlay, A.R. Hopscotch: A Fast Second-Order Partial Differential Equation Solver. *J. of the Inst. of Mathematics and its Apps* **1970**, 375–390.

9. Gourlay, A.R.; McGuire, G.R. General Hopscotch Algorithm for the Numerical Solution of Partial Differential Equations. *J. of the Inst. of Mathematics and its Apps* **1971**, 216–227.

10. Braband, J. Characterization of Evaporative Metal Bonding in Superalloys for Use in Gasified Coal Turbine Generators. M.S. Thesis, University of North Dakota, Grand Forks, ND, 2013.